



## A sensitive methane sensor of a ppt detection level using a mid-infrared interband cascade laser and a long-path multipass cell

Jinbao Xia<sup>a,b,c,\*</sup>, Chao Feng<sup>a,c,g</sup>, Feng Zhu<sup>d</sup>, Shuai Ye<sup>a</sup>, Sasa Zhang<sup>e</sup>, Alexandre Kolomenskii<sup>c,\*</sup>, Qiang Wang<sup>b,\*</sup>, Jian Dong<sup>c</sup>, Zhangjun Wang<sup>f</sup>, Wenling Jin<sup>b</sup>, Hans. A. Schuessler<sup>c</sup>

<sup>a</sup> State Key Laboratory of Crystal Materials, Shandong University, Jinan, 250100, China

<sup>b</sup> State Key Laboratory of Applied Optics, Changchun Institute of Optics, Fine Mechanics and Physics, Chinese Academy of Sciences Changchun, 130033, China

<sup>c</sup> Department of Physics and Astronomy, Texas A&M University, College Station, TX, 77843-4242, USA

<sup>d</sup> School of Physics and Astronomy, Sun Yat-sen University, Zhuhai, Guangdong, 519082, China

<sup>e</sup> School of Information Science and Engineering, and Shandong Provincial Key Laboratory of Laser Technology and Application, Shandong University, Qingdao, 266237, China

<sup>f</sup> Institute of Oceanographic Instrumentation, Qilu University of Technology (Shandong Academy of Sciences), Qingdao, Shandong, 266001, China

<sup>g</sup> Center for Optics Research and Engineering, Shandong University, Qingdao, 266237, China

### ARTICLE INFO

#### Keywords:

Wavelength modulation spectroscopy  
Wavelet denoising  
Multi-pass cell  
Allan deviation

### ABSTRACT

An ultra-high sensitivity sensor combining a mid-IR (MIR) interband cascade laser (ICL) at center wavelength of 3.37  $\mu\text{m}$  and a multi-pass cell (MPC) with a path-length of 580 m was designed and implemented for methane detection. The ultra-high sensitivity is achieved due to the higher absorbance in the MIR than in the near infrared (NIR), a long interaction path length, and the implementation of a wavelet denoising processing algorithm. The performance of the sensor was evaluated with direct absorption spectroscopy (DAS) and wavelength modulation spectroscopy (WMS) in a series of measurements. For the sensor working in the DAS measurement mode, the optimal set of sub-wavelet functions was chosen and utilized for denoising. A calibration gas with methane concentration of 2.0 ppm was measured with a relative error of  $\pm 1\%$ . The minimum of the Allan deviation of the sensor of 3 ppb was achieved with an averaging time of 200 s. For the WMS technique with the Allan deviation analysis the sensor detection limit for methane of 560 ppt with 290 s averaging time was determined, which is a significant improvement compared to our DAS results and previous reports. The developed sensor has broad applicability in the high-sensitivity measurements of methane and other trace gases.

### 1. Introduction

Methane is a highly potent greenhouse gas. As reported by the U.S. Environmental Protection Agency in 2017 [1], the methane emission accounted for over 10 % of all greenhouse gas emissions from human activities. The main sources of methane are seeps from natural gas systems, coal mines, and emissions related to industrial processes, livestock, and other agricultural practices [2,3]. Highly sensitive detection of methane is also important for biomedical applications, environmental monitoring, and the detection of leaks in the gas and oil industry. Compared to traditionally used chemical techniques, optical absorption spectroscopy provides the advantages of real-time, high resolution, and high sensitivity measurements. The theory of optical absorption

spectroscopy is based on the Beer-Lambert law for the light absorbed by atoms or molecules, which results in the transmission of light depending on the effective optical path in the sample and its absorption coefficient. The highly sensitive optical absorption spectroscopic techniques include wavelength modulation spectroscopy (WMS) [4,5], cavity ringdown spectroscopy (CRDS) [6], cavity-enhanced spectroscopy (CEAS) [7] and others. The methane sensor in the NIR wavelength interval around 1.65  $\mu\text{m}$  that we developed previously achieved ppb level for the detection limit [8]. For a sensor with even higher sensitivity at the ppt level, the NIR wavelengths are not optimal. The absorption cross-sections for methane are about two orders higher in the MIR wavelength range around 3.3  $\mu\text{m}$  than those in the NIR. In the MIR, such techniques as CRDS or CEAS can achieve even higher sensitivity by increasing the

\* Corresponding authors.

E-mail addresses: [xiajinbao413@163.com](mailto:xiajinbao413@163.com) (J. Xia), [alexandr@physics.tamu.edu](mailto:alexandr@physics.tamu.edu) (A. Kolomenskii), [wangqiang@ciomp.ac.cn](mailto:wangqiang@ciomp.ac.cn) (Q. Wang).

<https://doi.org/10.1016/j.snb.2021.129641>

Received 8 September 2020; Received in revised form 3 February 2021; Accepted 6 February 2021

Available online 14 February 2021

0925-4005/© 2021 Elsevier B.V. All rights reserved.

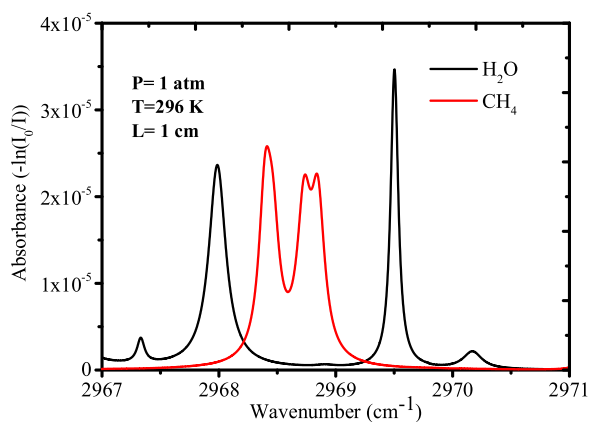


**Fig. 1.** The absorbance simulation with a 2 ppm concentration of  $\text{CH}_4$  and 1.6 % of  $\text{H}_2\text{O}$  under ambient air pressure, using a 1 cm path length and assuming Voigt line profile.

optical interaction path with high reflectivity mirrors. For low absorption, the effective optical path can be estimated as  $\sim L/(1-R)$ , where  $L$  is the distance between the two mirrors and  $R$  is the reflectivity. For the MIR sensors with CRDS or CEAS to achieve high sensitivity it is important to have ultrahigh reflectivity coatings of the mirrors and avoid their contamination since the latter can strongly reduce the effective interaction path. Also, for such resonance techniques, the reduction of vibrational noise should be implemented. To overcome these technical challenges, the combination of WMS and a multi-pass cell (MPC) is the preferred choice for trace gas detection in many practical applications. Many types of MPCs such as the White cell [9], the Herriot cell [10], the astigmatic Herriot cell [11] were reported over the past decades. With special design, the optical path of MPC can be increased to hundreds of meters. Various MIR MPC lengths were reported and used for trace gas detection: 18.3 m [12], 36.2 m [13], 89.6 m [14], 100 m [15,16]. Up to now, the longest reported optical path for

MIR MPC is  $\sim 240$  m [17]. There were several previous reports on the MIR methane sensors with MPC. In a proof of principle study in 2010, Tsai et al. reported a widely tunable external cavity ICL with a center wavelength of  $3.15 \mu\text{m}$  and showed the capability of detection of 2.2 % methane [18]. In 2016, Dong et al. developed a dual gas sensor with a CW ICL at a center wavelength of  $3.3 \mu\text{m}$  and a 54.6 m optical path MPC, achieving the detection limit of 11.2 ppb for methane with an averaging time of 3.4 s [19]. Davis et al. used an ICL and DAS with a gold-coated integrating sphere as a short gas cell with a length of 54.4 cm to measure methane with the detection limit of 1 ppm [20]. In 2018 Ye et al. developed a MIR methane sensor at  $3.293 \mu\text{m}$  with a 16 m optical path MPC [21], reaching the detection limit of 17.4 ppb.

In this work, to realize a longer path, we used the confocal principle to design an MPC with an optical path of 580 m, while the distance between the mirrors was 1 m. This MPC was tested and used for the development of a highly sensitive MIR methane sensor. The DAS and WMS approaches were used to measure the absorption and infer the methane concentration. For the DAS method, we evaluated the sub-wavelet functions for wavelet denoising of the signal [22] and extracted the absorption signal with the optimal wavelet function selection. Series of experiments were performed to assess the sensor performance. With DAS, the signal-to-noise-ratio (SNR) of 156 was determined with a standard calibration gas having a methane concentration of 2 ppm. The sensitivity of 3 ppb with an averaging time of 200 s was achieved. For the same conditions, the SNR with the WMS method increases to 3000. The detection limit of 560 ppt with the same calibration gas and an integration time of 290 s was achieved, thus enabling the ppt level of methane detection. We describe the sensor principle and design in Sections 2 and 3, present the results of performance tests in Section 4, and draw the conclusions in Section 5.

## 2. Wavelength coverage and detection principle

### 2.1. Wavelength tuning range and absorption line selection

The laser source used in this work is a commercial single-mode

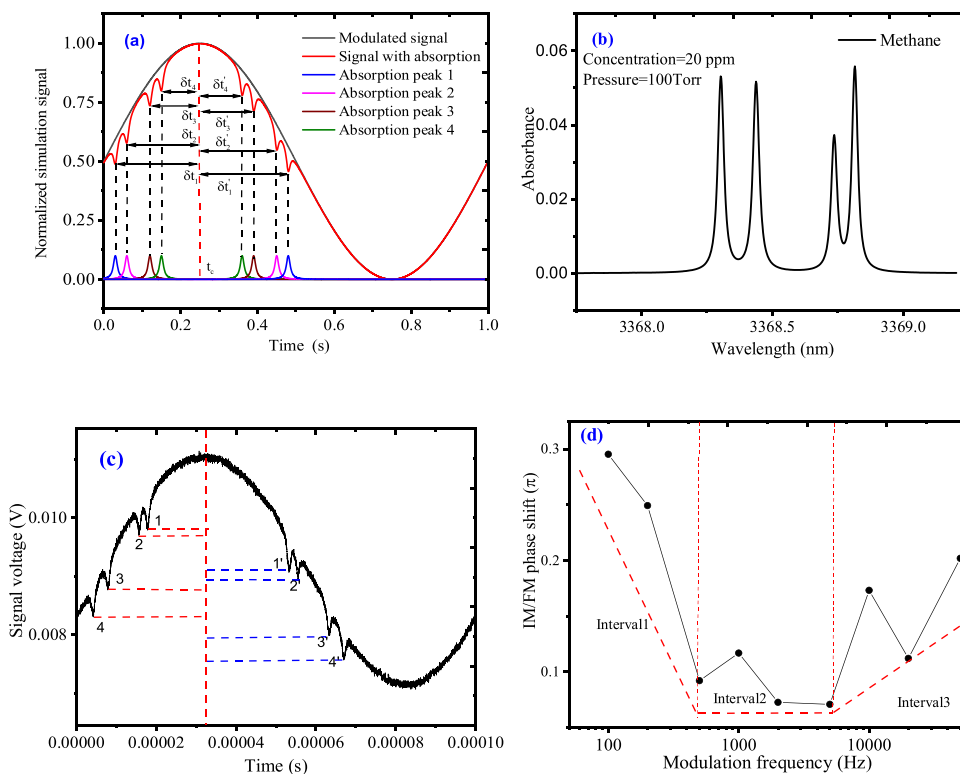


**Fig. 2.** The illustration of determining the IM/FM phase shift: (a) The simulated sine signal with four absorption peaks. (b) The methane absorption peaks: at relatively low pressure four well-separated peaks are obtained with the HITRAN database. (c) The four absorption peaks are detected in our experiment at the positive and negative slopes of the current scan. (d) The phase shift variations for different modulation frequencies. The red dotted line shows the borders of the frequency intervals with different trends of the variations of the IM/FM phase shift, as the modulation frequency is increasing.

continuous-wave ICL. The maximum output of the laser power was 10 mW at an injection current of 80 mA. The wavelength was measured by a spectrometer with a resolution of  $\sim 0.14 \text{ cm}^{-1}$  (Thermo Scientific Nicolet 8700 FT-IR, Thermo Fisher Inc.). The tunable wavelength range was from 3361 nm to 3372 nm covered by changing the laser current from 20 mA to 80 mA at three different temperatures  $10^\circ\text{C}$ ,  $15^\circ\text{C}$ , and  $20^\circ\text{C}$  (as shown in Fig.S1, see Supplementary Information).

The spectrum from  $3361 \text{ nm}$  ( $2971 \text{ cm}^{-1}$ ) to  $3372 \text{ nm}$  ( $2967 \text{ cm}^{-1}$ ) covers the absorption lines of both  $\text{H}_2\text{O}$  and  $\text{CH}_4$  (Fig. 1). The simulation in Fig. 1 for  $\text{H}_2\text{O}$  and  $\text{CH}_4$  absorbances is performed with the 2009 HITRAN database [23] for the conditions of 296 K temperature, 1 atm pressure, and 1 cm optical path-length with fractional volumes 1.6 % of  $\text{H}_2\text{O}$  and 2 ppm of  $\text{CH}_4$ . Voigt profiles of the water and methane absorption lines were assumed in this simulation. There are two strong water absorption lines and four methane lines ( $2968.40 \text{ cm}^{-1}$ ,  $2968.47 \text{ cm}^{-1}$ ,  $2968.73 \text{ cm}^{-1}$ ,  $2968.85 \text{ cm}^{-1}$ ) in the indicated wavelength interval. At room temperature and atmospheric pressure, the methane lines centered at  $2968.40 \text{ cm}^{-1}$  and  $2968.47 \text{ cm}^{-1}$  overlap; the lines at  $2968.73 \text{ cm}^{-1}$ ,  $2968.85 \text{ cm}^{-1}$  also partially overlap (we note that at low pressure the peaks are well separated, as is shown further in Fig. 2 (b)). The lines selected for methane measurements belong to the P-branch of the  $\nu_3$  rovibrational spectrum of methane [24]. These methane lines only slightly interfere with the water lines and therefore are suitable for methane detection.

## 2.2. Wavelength modulation spectroscopy and phase correction

WMS is a highly sensitive technique for trace gas detection [25]. It uses modulation of the laser injected current by the combination of a ramp voltage, tuning the wavelength over the absorption line region, and a higher frequency sine voltage, providing the signal that characterizes the absorption line. The signal of the transmission containing the gas concentration information is fed into a lock-in amplifier, and the second harmonic signal is extracted. The intensity and laser emission frequency are modulated as follows:

$$I(t) = \bar{I} + \Delta I \cos(\omega t + \psi), \quad (1)$$

$$\nu(t) = \bar{\nu} + \Delta \nu \cos(\omega t). \quad (2)$$

Here,  $\bar{I}$  is the average laser intensity, depending on the injected current,  $\Delta I$  is the modulation amplitude,  $\omega = 2\pi f$ , where  $f$  is the modulation frequency,  $\bar{\nu}$  is the average frequency of the laser,  $\Delta \nu$  is the frequency modulation amplitude,  $\psi$  is the phase shift between intensity modulation and frequency modulation (IM/FM). By the Beer-Lambert theory, the laser output intensity is expressed as  $I_0(t) = I(t) \exp[-\xi \varphi(\nu(t))]$ , where  $\xi = PXL_{op}S$ ,  $S = S(P, T)$  is the absorption line strength depending on the pressure,  $P$  and temperature,  $T$  of the gas,  $L_{op}$  is the optical path,  $\varphi(\nu, P, T)$  is the absorption line profile and  $X$  is the fractional concentration of the species of interest. The laser frequency  $\nu$  is oscillating while scanning the average frequency across the absorption line. Using Eqs. (1,2) with the Beer-Lambert equation for the transmitted light we obtain for the  $2f$ -signal after demodulation with the lock-in detection

$$S_{2f} = \frac{G\bar{I}}{2} \left\{ \left[ H_2 + \frac{\Delta I}{2I} (H_1 + H_3) \cos\psi \right]^2 + \left[ \frac{\Delta I}{2I} (H_1 - H_3) \sin\psi \right]^2 \right\}^{1/2}, \quad (3)$$

where  $G$  is a coefficient proportional to the system gain and the coefficients  $H_k$  ( $k$  is the harmonic index) can be expressed as

$$H_k(\bar{\nu}, \Delta \nu) = \frac{1}{2\pi} \int_{-\pi}^{\pi} \exp(-\xi \varphi(\bar{\nu} + \Delta \nu \cos(\theta))) \cos(k\theta) d\theta, k = 1, 2, 3, \dots \quad (4)$$

For a relatively small absorption,  $\xi \varphi(\nu(t)) \ll 1$ ,  $S_{2f}$  is proportional to the concentration of the species. However, Eqs. (4–5) describe also the case of significant absorption,  $\xi \varphi(\nu(t)) \geq 1$ , leading to a nonlinear

relation between the measured signal and gas concentration.

The importance of accurate accounting for the IM/FM phase shift follows from the fact that it always affects the detected signal in WMS through the residual amplitude modulation. To obtain the actual phase shift, the mirror reflection method by Lytkine et al. [26] and the time differences method by Liu et al. [27] were reported. We used the time differences method, which is relatively simple and allows us to improve the accuracy by using several absorption peaks.

The determination of the IM/FM phase shift is illustrated in Fig. 2(a), assuming that there are four absorption peaks within the scanning range. Each absorption peak labelled with certain color appears as a pair of dips in the signal: one on the slope of the increasing current and one on the falling slope. The black and red lines are the modulated current and modulated absorption signals, respectively. The average of four time-differences can be calculated as

$$\begin{aligned} \Delta t &= \frac{1}{2 \times 4} (\Delta t_1 + \Delta t_2 + \Delta t_3 + \Delta t_4) \\ &= \frac{1}{8} (\dot{t}_1 + t_1 + \dot{t}_2 + t_2 + \dot{t}_3 + t_3 + \dot{t}_4 + t_4 - 8t_c), \end{aligned} \quad (5)$$

where  $\Delta t_k = \delta t_k' - \delta t_k$  ( $k = 1, 2, 3, 4$ ) is the time difference for the  $k$ -th absorption peak pair;  $t_c$  is the central time at the maximum amplitude of the modulation signal, while  $\delta t_k' = t_k' - t_c$  and  $\delta t_k = t_c - t_k$  are time differences relative to  $t_c$  for the  $k$ -th pair of the signal dips (see Fig. 2(a)). The phase shift is then  $\psi = 2\pi f \Delta t$ . For an arbitrary number  $N$  of absorption peaks, the phase shift is proportional to the averaged time differences of pairs

$$\Delta t = \frac{1}{2N} \sum_{k=1}^N \Delta t_k. \quad (6)$$

In our experiment, we chose four methane absorption lines between 3368 nm and 3369 nm to find the IM/FM phase shift. The pressure in the chamber was lowered to 100 Torr to separate the overlapped methane lines. Four absorption peaks are simulated with the HITRAN database, as shown in Fig. 2(b). As depicted in Fig. 2(c), there are four pairs of the absorption peaks (1, 1'), (2, 2'), (3, 3'), (4, 4') in one full frequency scan.

To determine the frequency dependence of the phase shift (Fig. 2(d)), the driving current of the ICL-DFB laser was modulated by a voltage with different frequencies, and the data were acquired by an oscilloscope with a 100 MHz sampling rate (Tektronix MDO4104B-3). The phase shift is determined using Eq. (5). There are three modulation frequency intervals (separated by vertical red dashed lines) showing different behavior: (1) with the modulation frequency increasing from 100 Hz to 500 Hz, the phase shift decreases from  $0.3\pi$  to  $0.1\pi$ , (2) in the frequency interval from 500 Hz to 4 kHz the phase shift varies within the limits from  $0.07\pi$  to  $0.12\pi$ , and (3) above 5 kHz the phase shift increases, reaching  $\sim 0.2\pi$  at 50 kHz. The obtained IM/FM phase shift has similar trending to previously reported in Ref. [27], which also exhibited a significant phase delay at low frequency. The phase delay is produced due to the intrinsic properties of the laser itself. The ICL-DFB laser has the similar structure as the VCSELs reported by Hangauer et al. [28], which was packaged in a TO66 housing, including a thermoelectric cooler and a temperature coefficient thermistor. In the Interval 1 (Fig. 2 (d)) additional thermal resistance due to the contact of the laser chip and the submount contributes to the time delay. In the Interval 2, the effect of the laser chip submount is small. While in the Interval 3, the intrinsic thermal effect leads to the increase of the phase shift.

## 3. Mid-IR multipass cell and sensor design

The MIR MPC is designed on the principle of a confocal cavity. The radii of curvatures of the two  $50 \times 50 \text{ mm}^2$  mirrors are 1 m and equal to the distance between the two mirrors. Both mirrors are composed of 3 partitions, including two  $25 \times 25 \text{ mm}^2$  squares, and one  $25 \times 50 \text{ mm}^2$  rectangle. In one of the square partitions, a 5 mm diameter hole serves as

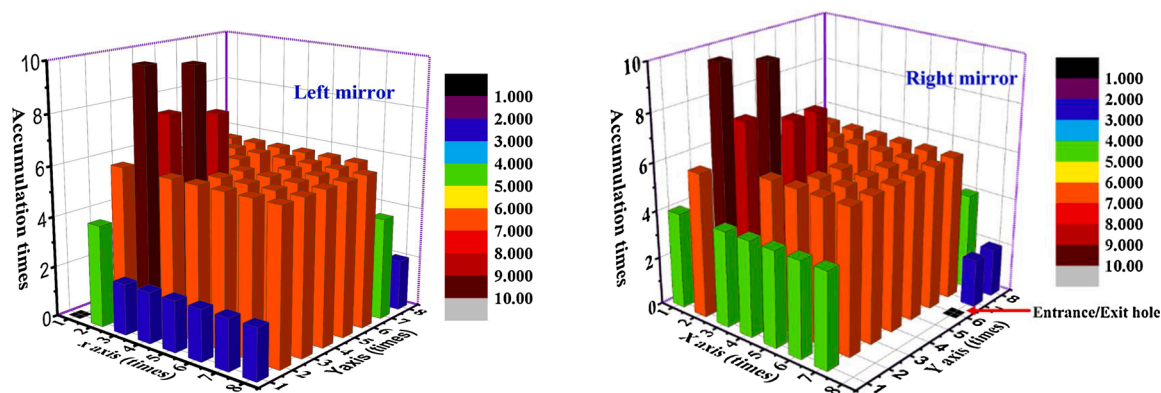


Fig. 3. The mirror image plot of the number of reflections from each subarea of the right and left mirrors.

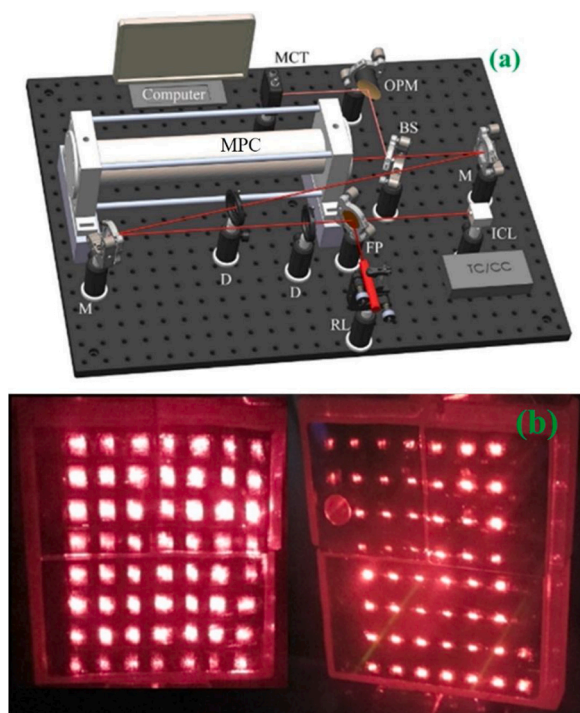


Fig. 4. (a) The schematic of the experimental setup of the methane sensor platform. ICL: distributed feedback interband cascade laser, MPC: multipass cell, M: plane mirror, BS: beam splitter, RL: red laser, OPM: off-axis parabolic mirror, MCT: HgCdTe detector, D: pinhole, TC/CC: temperature and current controller. FP: flip mirror. (b) The aligned spot distributions on the multipass mirrors. The spot brightness depends on the view angle and does not directly reflect the number of reflections.

the entrance and exit hole. The volume of the multi-pass cell is 2.5 L. The subsequent spots are aligned using the corresponding mirror mounts according to the performed simulation. After all six mirror partitions are aligned, the spot patterns are formed on the mirrors, and the laser beam exits the MPC (after bouncing between the mirrors) through the same hole it entered. The number of bounces for each spot can be different as the simulation shows (Fig. 3). The total number of reflections is 579, thus the effective path length is 580 m. The mirrors (Layertec GmbH) are coated for the MIR range assuring high reflectivity ( $>99.85\%$  for 3100–3600 nm).

The implementation of the MPC was realized as follows. A computer simulation code in MATLAB was developed to calculate a path with a large number of reflections. On each side the whole mirror arrangement was divided into 64 equal subareas, namely squares of  $6.25 \times 6.25 \text{ mm}^2$

size each. The simulation considered all subareas as the possible locations of the entrance and exit aperture. The program follows several optimization rules: each mirror side has its own center of curvature; each spot on the mirror is projected to the spot of the image position according to the optics of the curved mirror, from which the reflection took place. The calculation is performed in a loop finding the optimum sequence of reflections from the six mirrors with coordinates of each subsequent reflection determined by those from the previous reflection. The process continues until the beam exits through the same hole, from which it entered the system, and the appropriate configuration yielding the high number of reflections is obtained and used for adjusting the MPC. In calculation, the following restrains were imposed: the reflected beam cannot go outside the mirror areas, it must not go back to the edge of the incident aperture and must not be incident on the edges of the mirrors, the multi reflected beams must completely cover the volume of the MPC. In cases in which the beam leaves the surface of the mirrors, the simulation is terminated, and new locations and orientations of curvatures are assigned. The finding of the configuration with 579 reflections in the MPC took about two days on a personal computer. With calculated sequence of reflections and spot configuration, the mirrors were adjusted accordingly, and after correct positioning of certain number of reflection spots (typically less than  $\sim 20$ ) the desired configuration corresponding to the calculated one was achieved (see also Supplementary Information, Figs. S2,S3).

Based on the MIR MPC, we designed a highly sensitive sensor, as shown in Fig. 4. The MIR laser is controlled by a commercial laser current and temperature controller (ILX Lightwave, LDC-3724). The output from the ICL-DFB was injected into the MPC with two mirrors. After bouncing in the MPC the laser beam was reflected by a beam splitter and focused by an off-axis parabolic mirror with a focal length of  $f = 10.2 \text{ cm}$  on a four-stage thermoelectrically cooled MCT photodetector (Mercury Cadmium Telluride, Vigo, PIP-DC-20M-F-M4) with a bandwidth of 15 MHz. To control spectral measurements a LabVIEW program based on the DAQ software with a multifunction I/O device (National Instruments, USB6361) was developed. The program controls the laser scanning and modulation, data acquisition, demodulation, lock-in amplification, and saving of the data. A detailed description of the software was presented in our previous work [8]. For the alignment, we first used a visible red diode laser to adjust the multi-pass mirrors and to achieve the simulated spot patterns, as shown in Fig. 4(b). Then the MIR beam replaced the red laser beam by turning up the flip mirror and was aligned through two pinholes to enter the MPC. The output of the MPC was around  $10 \mu\text{W}$ , which depended on the humidity because of the large water vapor absorption.

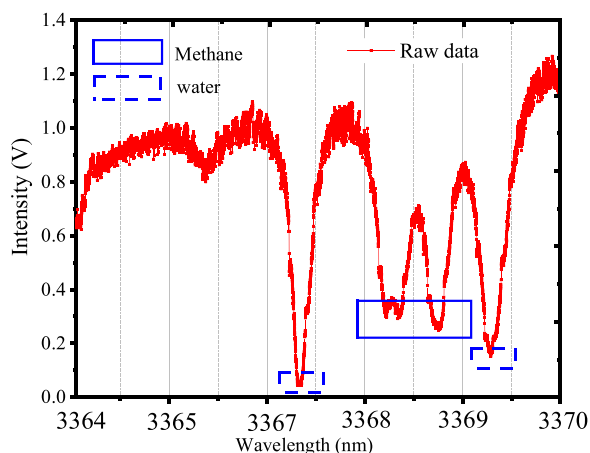


Fig. 5. The raw data acquired in the DAS measurement. Methane peaks are labelled with a solid box, and water peaks are shown with dashed boxes.

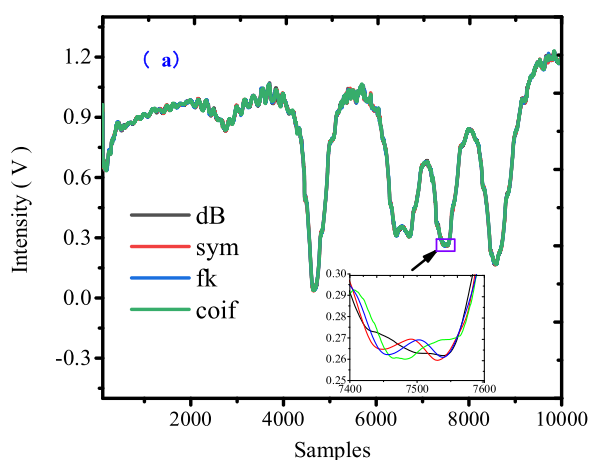


Fig. 6. The comparison of four sets of subwavelet functions for denoising of the signal.

## 4. Experimental results

### 4.1. Direct absorption spectroscopy measurement and data processing

In the DAS experiment, to assess the performance of the sensor we used the standard calibration gas with a methane concentration of 2 ppm from the GASCO company. The scanning voltage of the laser was a sawtooth wave with a peak-to-peak value of  $\sim 2$  V from 6 V to 8 V, corresponding to the input current from 60 mA to 80 mA, and a frequency of 1 Hz. The raw signal was acquired by a data acquisition card (National Instruments USB 6361) with a sampling rate of 10 kHz. We first flushed the MPC with pure nitrogen for about thirty minutes until only the background signal was left and then filled it with the methane calibration gas. The strong absorption signals for  $\text{H}_2\text{O}$  and  $\text{CH}_4$  were acquired, as shown in Fig. 5. The signal exhibited some fringes due to the optical etaloning effect. The fringes are mainly caused by spurious reflections in the MPC. The intensity of the fringe noise varied sinusoidally with changing the laser frequency. The magnitude of this fringe noise is usually larger than from other noise sources, such as laser intensity fluctuations or the shot noise of the photodiode. The free spectral range (FSR) was calculated with the confocal equation  $\text{FSR} = C/4L = 75$  MHz, where  $L$  is the length between the two mirrors of the MPC. These fringes are responsible for the noise in the plot, but can be suppressed in some approaches, such as wavelength modulation spectroscopy or frequency modulation spectroscopy.

To get the precise signal the procedures of signal denoising, baseline removal and signal fitting were applied to the absorption raw data. For signal processing the wavelet denoising method based on the denoising package from MATLAB 2019 was used, and a more detailed description of its implementation is presented in Ref. [29]. Wavelet denoising is an efficient method to remove noise, and it has been widely used in the TDLAS sensors [22]. The basic idea of this method is to decompose the signal into the sum of sub-wavelet functions with some coefficients. After the coefficients are filtered using a certain threshold frequency value, the signal is recombined with these filtered coefficients. Generally, the wavelet functions, such as dB, sym, fk, and coif were used in the wavelet analysis. Different function sets show different performance. We employed wavelet denoising with four sets of wavelet functions applied to the raw data, and the results are shown in Fig. 6. From the comparison, we have chosen the optimal set of dB9 wavelet functions at the decomposition level of 6 to remove the noise in the data.

After the signal was denoised with the wavelet method, the absorption signal was further refined by the baseline removal, as shown in Fig. 7(a). The standard deviation in the interval within the

blue dashed lines with no methane absorption (the base noise) in Fig. 7(a) was calculated resulting in the value of 0.0053 V. The signal amplitude for the selected absorption peak of methane at  $3.37 \mu\text{m}$  (within vertical blue dashed lines) is 0.87 V. Consequently, the SNR was calculated to be 164, i.e.  $\sim 44$  dB. The selected absorption peak was measured for twenty minutes, and fitting of different acquisitions provided the methane concentration values with some distribution. The histogram of this distribution is shown in Fig. 7(c). It can be well fitted by a Gaussian distribution with the HWHM of 30 ppb, also shown in Fig. 7(c) by a red line. The standard deviation ( $1\sigma$ ) of the concentration measurement is 20 ppb. Thus, for the  $\text{CH}_4$  concentration value of 2 ppm, the relative error (uncertainty of the measurement) is  $\pm 1\%$ . The sensor detection limit was determined to be 3 ppb with an averaging time of 200 s by the Allan deviation analysis [30,31], as shown in Fig. 7(d).

### 4.2. Wavelength modulation spectroscopy measurements

To improve the sensitivity of the sensor we employed the WMS technique. We realized this method similarly to previously reported work [8] based on LabVIEW program, which included ramp and sine signal generation, data acquisition and data demodulation. The wavelength was scanned by applying a sine voltage with a peak-to-peak value of 1 V from 6.5 V to 7.5 V and a frequency of 1 Hz and the sine modulation voltage at a frequency of 10 kHz and amplitude of 0.15 V corresponding to the input current of 15 mA from the DAQ card (NI, USB-6361). The output voltage first went into a home-made voltage follower, increasing the impedance, and then it was sent to the laser controller (ILX Lightwave, LDC-3724) to modulate the laser current. The IM/FM phase shift  $\psi$  was determined to be  $0.08\pi$ , based on measurements of the time delays and Eq. (6). The 20 kHz sine signal was also generated by the LabVIEW-based software to extract the second harmonic from the absorption signal measured with the photodetector. The second harmonic signal of  $\text{H}_2\text{O}$  and  $\text{CH}_4$  is shown in Fig. 8(a). The SNR of the signal is  $\sim 3000$ , i.e. 70 dB or  $\sim 20$ -fold improvement compared to the DAS method. To establish the relationship between the signal amplitude and methane concentration the sensor was calibrated with the calibration gas in the MPC. The overall dependence up to a concentration of 3 ppm was also calculated with Eqs. (1–4) and is shown in Fig. 8(b). For methane concentration less than 0.25 ppm (the signal amplitude  $\leq 0.0093$  V) a linear relationship with an error of less than 1% takes place  $C = 27.0 \times V_{2f}$  (ppm), where  $C$  is the concentration of methane with unit of ppm and  $V_{2f}$  is the measured 2f-signal amplitude with unit of Volt; for higher concentrations a nonlinear sensor response takes place. The WMS measurement was continued for twenty minutes at a 1 Hz sampling rate, acquiring a total of 1200 sampling points, shown in Fig. 9(a). The standard deviation ( $1\sigma$ ) for this data is 8 ppb, about 3-fold improvement compared to the DAS method. The Allan deviation

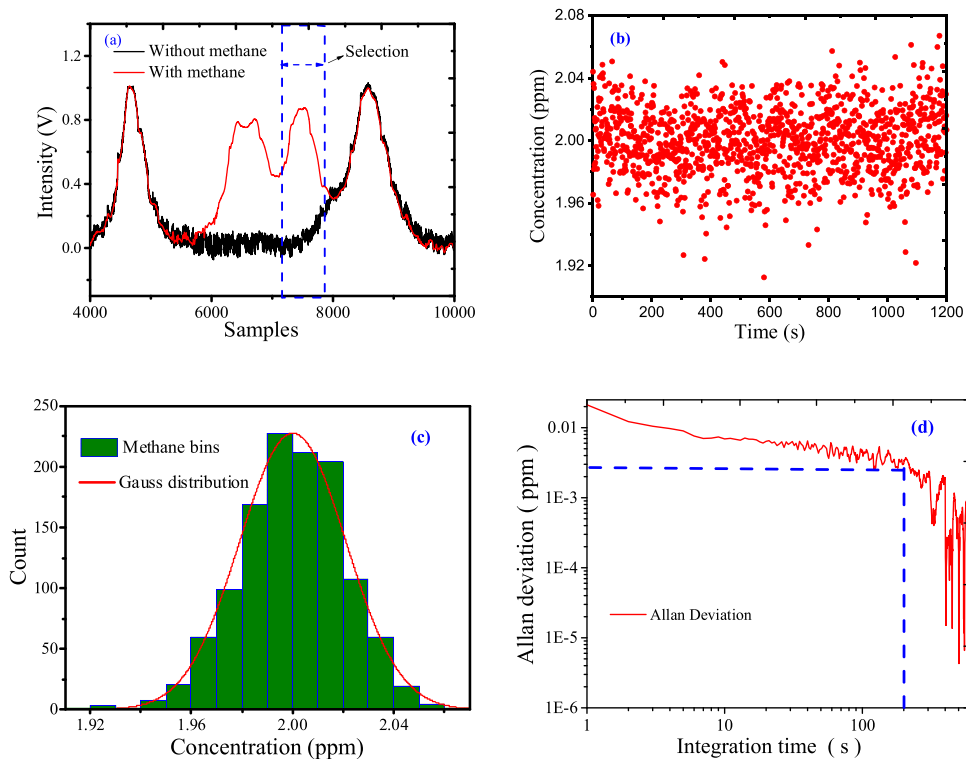


**Fig. 7.** (a) Methane absorption signal (b) Methane concentrations determined from the measurement for twenty minutes. (c) The Gaussian distribution of the methane concentration measurement. (d) Allan deviation analysis of the DAS methane measurement.

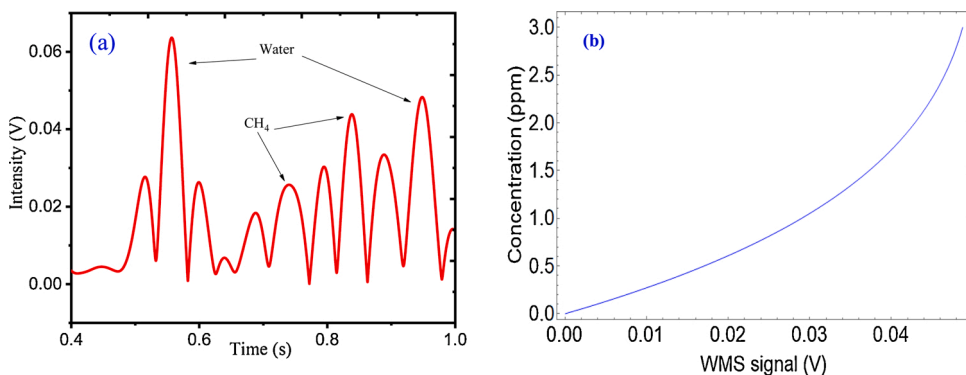


**Fig. 8.** The second harmonic signal of methane and water (a) and the calculated dependence of methane concentration on the amplitude of the measured signal (b).

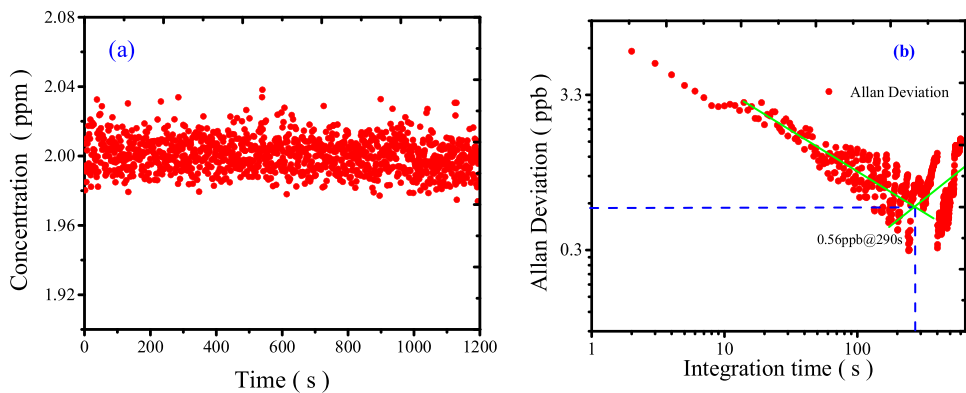


**Fig. 9.** The results for WMS measurements: (a) Methane concentrations for 1200 sampling points obtained in twenty minutes of continuous measurement. (b) The Allan deviation analysis of the measurement results.

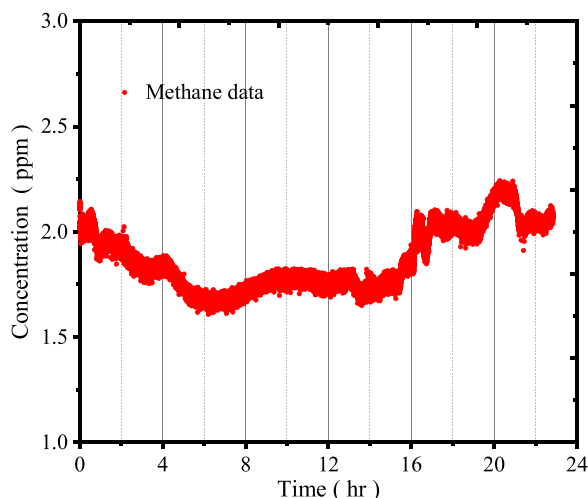


Fig. 10. Long-time measurement for methane.

analysis is presented in Fig.9(b). We fitted the Allan deviation of data from 20 s to 300 s by a line with a descending slope in Fig. 9(b), and also fitted the Allan deviation data from 200 s to 500 s. The middle line minimum of the Allan deviation was determined by the crossing point of the two fitting lines. Consequently, we obtained the detection limit of 560 ppt with 290 s averaging time, corresponding to minimum detectable absorption coefficient of  $7.2 \times 10^{-9} \text{ cm}^{-1}$ .

Also, we carried out a long-time measurement of the ambient air for  $\sim 24$  h (Fig. 10). The data were acquired at the scanning rate of 1 Hz, modulation frequency of 10 kHz, and sampling rate of 100KHz. During this long measurement the setup was in the indoor environment with temperature variations  $\leq 1^\circ\text{K}$ . The estimates show that even temperature variations as large as  $\sim 7^\circ\text{K}$  induce signal variations, which are less than the detection limit. The methane concentration decreased with time from 2.02 ppm to about 1.60 ppm and then increased to  $\sim 2.02$  ppm again.

## 5. Discussion and summary

In this paper, we designed a mid-IR multipass cell with an optical path of 580 m, which is the longest optical path in the MIR reported to date. We built a sensitive methane sensor and used two measuring methods of direct absorption spectroscopy (DAS) and wavelength modulation spectroscopy (WMS). With the first method, in the measurement of methane in atmospheric air, the signal with the high signal-to-noise-ratio (SNR) of 44 dB and the sensitivity of 3 ppb with an averaging time of 200 s was achieved using the wavelet denoising method. The measured concentration of  $\sim 2$  ppm had a standard deviation of 2.5 % and an Allan deviation of 3 ppb. The sensitivity of the sensor was further improved with the WMS technique. Within this approach, we used four methane absorption lines to determine the phase shift between the intensity modulation and frequency modulation. With the WMS method, the SNR was increased to 70 dB and the detection limit of 560 ppt was achieved with an averaging time of 290 s, thus permitting the ppt level of methane detection.

## Contribution-statement

**Jinbao Xia**, Conceptualization; Investigation, Roles/Writing – original draft

Investigated the idea, Carried out the experiment and writing the original draft

**Feng Zhu**, Methodology;

Designed the multipass cell in MIR

**Alexandre Kolomenskii**, Writing – review & editing, Methodology,

Validation;

Writing and validating the paper

**Shuai Ye**, Visualization;

Produced the figure of the experimental setup as a 3D visualization.

**Sasa Zhang**, Project administration

Initiated the experiment

**Chao Feng**, Data curation

Data analysis maintaining the data

**Qiang Wang**, Funding acquisition;

Facilitated the open funding

**Jian Dong**, Software development

**Zhangjun Wang**, Software development

Developed data analysis algorithm

**Hans. A. Schuessler**, Resources & supervision

Supervised and provided resources

## Declaration of Competing Interest

The authors have no any financial relationship that might be construed as a conflict of interest that can influence the results or interpretation of the results of this article.

## Acknowledgments

This work was supported by the Robert A. Welch Foundation, grant No. A1546, and National Science Foundation of Shandong Province (ZR2018BF030), International Postdoctoral Exchange Fellowship Program (2018065), Open Fund of State Key Laboratory of Applied Optics (SKLA02020001A12), National Key Research and Development Project (2016YFC1400301, 2018YFC1407300), Shandong Provincial Key Research and Development Project (2019GGX104004), Opening Foundation of Shandong Provincial Key Laboratory of Laser Technology and Application.

## Appendix A. Supplementary data

Supplementary material related to this article can be found, in the online version, at doi:<https://doi.org/10.1016/j.snb.2021.129641>.

## References

- <https://www.epa.gov/>.
- Z.M. Ji, Z.J. Chen, J.N. Pan, Q.H. Niu, A novel method for estimating methane emissions from underground coal mines: the Yanma coal mine, China, *Atmos. Environ.* 170 (2017) 96–107.
- K. Minami, K. Takata, Atmospheric methane: sources, sinks, and strategies for reducing agricultural emissions, *Water Sci. Technol.* 36 (1997) 509–516.
- L.C. Philippe, R.K. Hanson, Laser diode wavelength-modulation spectroscopy for simultaneous measurement of temperature, pressure, and velocity in shock-heated oxygen flows, *Pure Appl. Opt. J. Eur. Opt. Soc. Part A* 32 (30) (1993) 6090–6993.
- A. Behera, A.B. Wang, Calibration-free wavelength modulation spectroscopy: symmetry approach and residual amplitude modulation, *Pure Appl. Opt. J. Eur. Opt. Soc. Part A* 55 (16) (2016) 4446–4455.
- E.R. Crosson, A cavity ring-down analyzer for measuring atmospheric levels of methane, carbon dioxide, and water vapor, *Appl. Phys. B: Lasers Opt* 92 (2008) 403–408.
- S.E. Fiedler, A. Hese, A.A. Ruth, Incoherent broad-band cavity-enhanced absorption spectroscopy, *Chem. Phys. Lett* 371 (3–4) (2003) 284–294.
- J. Xia, F. Zhu, S. Zhang, A.A. Kolomenskii, H.A. Schuessler, A ppb level-sensitive sensor for atmospheric methane detection, *Infrared Phys. Technol.* 86 (2017) 194–201.
- R.G. Pilston, J.U. White, A long path gas absorption cell, *J. Opt. Soc. Am.* 44 (1954) 572–573.
- D. Herriot, H. Kogelnik, R. Kompfner, Off-axis paths in spherical mirror interferometers, *Appl. Opt.* 3 (1964) 523–526.
- J.B. McManus, P.L. Kebabian, M.S. Zahniser, Astigmatic mirror multipass absorption cells for long-path-length spectroscopy, *Appl. Opt.* 34 (1995) 3336–3348.
- Y. Mine, N. Melander, D. Richter, D.G. Lancaster, K.P. Petrov, R. F. Curl, F.K. Tittel, Detection of formaldehyde using mid-infrared difference-frequency generation, *Appl. Phys. B* 65 (1997) 771–774.

- [13] M. Seiter, M.W. Sigrist, Trace-gas sensor based on mid-IR difference-frequency generation in PPLN with saturated output power, *Infrared Phys. Technol.* 41 (2000) 259–269.
- [14] D. Richter, P. Weibring, J.G. Walega, A. Fried, S.M. Spuler, M.S. Taubman, Compact highly sensitive multi-species airborne midIR spectrometer, *Appl. Phys. B* 119 (2015) 119–131.
- [15] D. Rehle, D. Leleux, M. Erdelyi, F. Tittel, M. Fraser, S. Friedfeld, Ambient formaldehyde detection with a laser spectrometer based on difference-frequency generation in PPLN, *Appl. Phys. B* 72 (2001) 947–952.
- [16] P. Weibring, D. Richter, A. Fried, J.G. Walega, C. Dyroff, Ultrahigh-precision mid-IR spectrometer II: system description and spectroscopic performance, *Appl. Phys. B* 85 (2006) 207–218.
- [17] J.B. McManus, M.S. Zahniser, D.D. Nelson, Dual quantum cascade laser trace gas instrument with astigmatic Herriott cell at high pass number, *Appl. Opt.* 50 (2011) 74–85.
- [18] T.R. Tsai, et al., Widely tunable external cavity interband cascade laser for spectroscopic applications. *CLEO/QELS: 2010 Laser Science to Photonic Applications*, San Jose, CA, 2010, pp. 1–2.
- [19] L. Dong, F.K. Tittel, C. Li, Nancy, P. Sanchez, H. Wu, C. Zheng, Y. Yu, A. Sampaolo, R.J. Griffin, Compact TDLAS based sensor design using interband cascade lasers for mid-IR trace gas sensing, *Opt. Express* 24 (2016) 528–535.
- [20] N.M. Davis, J. Hodgkinson, D. Francis, R.P. Tatam, Sensitive detection of methane at 3.3  $\mu\text{m}$  using an integrating sphere and interband Cascade laser, *Conference on Optical Sensing and Detection IV*, Proceedings of SPIE (2016).
- [21] W. Ye, C. Li, C. Zheng, N.P. Sanchez, A.K. Gluszek, A.J. Hudzikowski, L. Dong, R. J. Griffin, F.K. Tittel, Mid-infrared dual-gas sensor for simultaneous detection of methane and ethane using a single continuous-wave interband cascade laser, *Opt. Express* 24 (2016) 16973–16985.
- [22] C.T. Zheng, W. Ye, J. Huang, T. Cao, M. Lv, J.M. Dang, Y.D. Wang, Performance improvement of a near-infrared CH<sub>4</sub> detection device using wavelet-denoising-assisted wavelength modulation technique, *Sens. Actuators B Chem.* 190 (2014) 249–258.
- [23] L.S. Rothman, I.E. Gordon, Y. Babikov, A. Barbe, D. Chris Benner, P.F. Bernath, et al., HITRAN2012 molecular spectroscopic database, *J. Quant. Spectrosc. Radiat. Transfer* 130 (2013) 4–50.
- [24] M. Alrefae, E. Es-sebbar, A. Farooq, Absorption cross-section measurements of methane, ethane, ethylene and methanol at high temperatures, *J. Mol. Spectrosc.* 303 (2014) 8–14.
- [25] J.Y. Li, G. Luo, Z.H. Du, Y.W. Ma, Hollow waveguide enhanced dimethyl sulfide sensor based on a 3.3  $\mu\text{m}$  interband cascade laser, *Sens. Actuators B Chem.* 255 (2018) 3550–3557.
- [26] A. Lytkine, W. Jäger, J. Tulip, Long-wavelength VCSELs for applications in absorption spectroscopy: tuning rates and modulation performances, *Proc. SPIE. Int. Soc. Opt. Eng.* 5737 (2005) 157–166.
- [27] (a) Y.N. Liu, J. Chang, J. Liu, J. Liu, Q. Wang, C.G. Zhu, A time difference method for measurement of phase shift between distributed feedback laser diode (DFB-LD) output wavelength and intensity, *Sensors* 15 (2015) 16153–16161; (b) J. Li, Z. Du, Y. An, Frequency modulation characteristics for interband cascade lasers emitting at 3  $\mu\text{m}$ , *Appl. Phys. B* 121 (2015) 7–17.
- [28] A. Hangauer, J. Chen, R. Strzoda, M.C. Amann, The frequency modulation response of vertical-cavity surface-emitting lasers: experiment and theory, *IEEE J. Sel. Top. Quantum Electron.* 17 (2012) 1584–1593.
- [29] J. Xia, C. Feng, F. Zhu, S. Zhang, A. Kolomenskii, J. Dong, H.A. Schuessler, Real-time measurement of methane in a turbulent atmosphere over kilometer long paths with denoising methods, *Measurement* 168 (2021), 108467.
- [30] P. Werle, R. Mücke, F. Slemr, The limits of signal averaging in atmospheric trace-gas monitoring by tunable diode-laser absorption spectroscopy (TDLAS), *Applied Physics B* 57 (1993) 131–139.
- [31] G. Jacobson, C. Rella, A. Farinas, Application of Allan Deviation to assessing uncertainties of continuous-measurement instruments, and optimizing calibration schemes, *Geophys. Res. Abstr.* 16 (2014). EGU2014-15823.

**Jinbao Xia** received his master's degree from Ocean University of China in 2010. He obtained his PhD degree from the Institute of Science and Technology, Shandong University and also performed his research visiting Texas A&M University. Now he works as a postdoc. His scientific interests include trace gas detection and laser remote sensing.

**Chao Feng** received his B.S. and M.S. degrees from the College of Physics and Electronics Science, Shandong Normal University, Jinan, China, in 2010 and 2013, respectively, and the Ph.D. degree from the Advanced Research Center for Optics, Shandong University, Jinan, China, in 2017. He is currently a postdoc with the State Key Laboratory of Crystal Materials, Shandong University. He performed his research visiting Texas A&M University in 2018–2020. His research interests include novel laser materials, ultrafast laser, and solid-state lasers.

**Feng Zhu** received his PhD degree from Texas A&M University (TAMU) in 2010 performing his research in the SIBOR laboratory of TAMU, where he also worked as a postdoc. Now he is an associate professor at the School of Physics and Astronomy, Sun Yat-sen University (China), and his scientific interests are ion traps, frequency comb, and laser diode spectroscopies and trace gas detection.

**Shuai Ye** received his Bachelor's Degree in Science, from College of Science, Qilu University of Technology in 2018. He is now a PhD candidate in Shandong University. His current research interests include solid mid-infrared lasers, the design of optical and spectroscopic detection systems and trace gas detection.

**Sasa Zhang** is currently a Professor and Doctoral Supervisor at School of Information Science and Engineering, Shandong University. He graduated from Optics Department of Shandong University in 1986 and received his PhD from School of Information Science and Engineering, Shandong University in 2008. His main research interests focus on laser technology, optical sensing, trace gas analysis with neural network and deep learning, remote sensing for gas detection, spectrum technology and application, nano-materials simulation and fabrication.

**Alexandre Kolomenskii** received his PhD degree from P. N. Lebedev Physical Institute of the Russian Academy of Sciences in 1980. Now he is a Research Scientist at Texas A&M University. His fields of scientific interests include applications of lasers in acoustics, spectroscopy, and ultrafast laser interactions with atomic and molecular systems.

**Qiang Wang** is currently an associate professor in the State Key Laboratory of Applied Optics at Changchun Institute of Optics, Fine Mechanics and Physics, Chinese Academy of Sciences. He received his B.S. degree in Electronic Science and Technology in 2011 and Ph.D. degree in Optical Engineering in 2016 from Shandong University. After his graduate study, he worked as a postdoctoral fellow at the Chinese University of Hong Kong and Max Planck Institute of Quantum Optics successively. His recent research interests include laser spectroscopy, optical sensing, and engineering application of trace gas analysis in atmosphere, deep sea, and public health.

**Jian Dong** received his MS degree from Beijing University of Technology in 2017. Now he is a PhD student at Texas A&M University. His research areas are high order harmonic generation in gases and solids and spectroscopy.

**Zhangjun Wang** received his PhD degree in Ocean Information Detection and Processing, from the Ocean University of China in 2011. He is now working as an associate professor in the Institute of Oceanographic Instrumentation, Qilu University of Technology (Shandong Academy of Sciences). His current research interests include the design of atmospheric and marine Lidar systems.

**Wenling Jin** received her master's degree in Optics from Changchun Institute of Optics, Fine Mechanics and Physics (CIOMP), Chinese Academy of Sciences in 2020. She is now working as a research assistant in the State Key Laboratory of Applied Optics at CIOMP. Her current research interests include the design of optical and spectroscopic detection systems and trace gas detection.

**Hans Schuessler** is a Professor of Physics at the department of Physics & Astronomy of Texas A&M University. He received his PhD degree at Heidelberg University in 1964. His research fields include ion traps, laser spectroscopy and its applications, ultrafast laser phenomena and high sensitivity detection of trace gases.